Journal of Materials Processing Tech. 287 (2021) 116659

Contents lists available at ScienceDirect

Journal of Materials Processing Tech.

journal homepage: www.elsevier.com/locate/jmatprotec

Theory of single point incremental forming of tubes

V.A. Cristino[a], J.P. Magrinho[b], G. Centeno[c], M.B. Silva[b], P.A.F. Martins[b,*]

[a] Department of Electromechanical Engineering, University of Macau, Avenida da Universidade, Taipa, Macao
[b] IDMEC, Instituto Superior Tecnico, Universidade de Lisboa, Av. Rovisco Pais, 1049-001, Lisboa, Portugal
[c] Department of Mechanical and Manufacturing Engineering, University of Seville, Camino de los Descubrimientos, 41092 Seville, Spain

ARTICLE INFO

Associate Editor: Guest Exeter

Keywords:
Single point incremental forming
Tubes
Deformation mechanics
Membrane analysis
Experimentation

ABSTRACT

Knowledge of the deformation mechanics in single point incremental forming of tubes is of great importance to understand the physics behind failure and the workability limits in thin-walled tube expansion. Which are the states of stress and strain in the small localized plastic deformation region between the tube and the single point forming tool, and how damage accumulates until fracture are important questions that this paper seeks to address by means of an analytical model based on membrane analysis. Comparisons are made against conventional tube expansion with a rigid punch to explore the main differences between the two processes regarding the states of stress and strain, the accumulation of damage and the likely mode of failure. The investigation is supported by experimentation performed in aluminium AA6063-T6 and shows that differences in deformation mechanics allow incremental tube expansion to withstand slightly higher values of damage before cracking than conventional tube expansion.

1. Introduction

The past years have witnessed a growing academic and industrial interest in the development and utilization of incremental forming processes. Incremental forming processes contrary to well-established conventional forming processes, are especially adjusted to current industrial trends towards agile manufacturing for staying responsive to evolving customer demands and to meet the needs for greater product customization and shorter development and fabrication times.

Incremental forming of sheets and plates was most likely one of the manufacturing processes that has received more attention from researchers in the last two decades. The number of research publications in the field is large and covers a wide range of topics from deformation mechanics, formability limits and geometrical accuracy to equipment and applications (Duflou et al., 2018).

In contrast to incremental sheet forming, the work on incremental tube forming has been scarce and limited to a few number of research publications. The first pioneering work was performed in the mid 1990's by Matsubara (1994), who utilized a single point hemispherical tool with a numerically controlled tool path to shape the open end of tubes into various axisymmetric and polygonal geometries.

Unlike spinning that performs incremental tube forming under rotation in dedicated machine-tools (Kalpakjian and Rajagopal, 1982), the process introduced by Matsubara resembles single point incremental forming of sheets. This is because the tool follows a numerically controlled path to progressively shape the end of fixed (non-rotating) tubes without support from backup dies or mandrels. This paper is focused on this process and another interesting development was made by Teramae et al. (2007) who utilized a conical tool to produce hole flanges for tube branching applications. Finite element modelling and experiments helped understanding the influence of material strain hardening and anisotropy on the final tube wall thickness.

Subsequent work by Wen et al. (2015) recovered the idea of utilizing a single point hemispherical tool to perform expansion and reduction of tube ends as well as tube wall grooving and hole-flanging. Force, wall thickness and geometry were investigated for different operating parameters. Wen et al. (2017) later replaced the hemispherical tool by a conical tool to extend incremental forming to external and internal inversion of tube ends. The work involved experimentation and numerical simulation to identify major failures resulting from different operating conditions and to prove the overall feasibility of the process.

Recently, Movahedinia et al. (2018) focused on the expansion by incremental tube forming (hereafter designated as 'incremental tube expansion') and presented a comprehensive numerical and experimental investigation on the influence of different forming strategies on the maximum achievable inclination of the tube ends. The influence of

* Corresponding author.
E-mail addresses: vcristino@umac.mo (V.A. Cristino), joao.magrinho@tecnico.ulisboa.pt (J.P. Magrinho), gaceba@us.es (G. Centeno), beatriz.silva@tecnico.ulisboa.pt (M.B. Silva), pmartins@tecnico.ulisboa.pt (P.A.F. Martins).

https://doi.org/10.1016/j.jmatprotec.2020.116659
Received 25 February 2019; Received in revised form 8 January 2020; Accepted 21 February 2020
Available online 22 February 2020
0924-0136/

the main operating parameters on tube wall thickness and maximum attainable strains were supported by experimental measurements.

Similarly to what authors did in incremental sheet forming a couple of years ago (Silva et al., 2008b), it is the purpose of this paper to present the first analytical model that is capable of explaining the fundamentals of incremental tube expansion and the main differences against conventional tube expansion with a rigid punch. Although the analytical model will also be built upon membrane analysis and free body equilibrium of a local shell element along the three principal directions under rigid perfectly plastic material flow conditions, there will be significant differences against that of Silva et al. (2008b). This is because the workpieces are tubes instead of sheets, and the boundary conditions and strain loading paths are specific of incremental tube expansion instead of incremental sheet forming.

The model is constructed for rotationally symmetric conditions and major assumptions related to deformation modes and strain loading paths are validated by experimentation in conventional and incremental expansion of commercial aluminium AA6063-T6 tubes. Besides addressing the deformation mechanics of incremental tube expansion and the associated states of stress and strain, the presentation is also focused on explaining the physics behind failure and to quantify the critical ductile damage at the onset of cracking. Strain measurements using digital image correlation and circle grid analysis give support to the overall conclusions.

2. Theoretical background

2.1. General assumptions

The analytical model for incremental tube expansion is built upon membrane analysis (Fig. 1) and its derivation is based on an extension to tubes of the approach that has been employed by the authors for the incremental forming of sheets and plates (Silva et al., 2008a).

Fig. 1a shows a schematic representation of incremental tube expansion in which the contact area conforms to the hemispherical shape of the tool and is characterized by the local shell element ABCD plotted in dark grey (Fig. 1a). The local shell element delimits the instantaneous plastically deforming region of the tube subjected to normal forces, shear forces and bending moments.

The normal to the local shell element ABCD cuts the z-axis at point O and r_2 is the corresponding radius (Fig. 1c). The centre of curvature of the local shell element is located at point Q and r_1 is the radius of curvature along the meridian direction (Fig. 1c). The radius of curvature r_1 is identical to the tool radius $r_1 = r_{tool}$ because the local shell element is assumed to conform to the hemispherical shape of the tool.

The states of stress and strain, and the accumulation of ductile damage in the local shell element are derived from the membrane equilibrium conditions under the assumption of rotating symmetry plasticity. Further simplifications consist in the assumption that (i) material is isotropic and rigid-perfectly plastic, (ii) bending moments can be neglected, (iii) friction stresses are small enough for the circumferential, meridional and thickness stresses to be considered as principal stresses and (iv) frictional effects may be split in meridional $\mu_\phi \sigma_t$ and circumferential $\mu_\theta \sigma_t$ stress components (Fig. 1d).

The free body equilibrium of the local shell element ABCD of Fig. 1 is also applied to conventional tube expansion with a rigid tapered conical punch (hereafter designated as 'conventional tube expansion', Fig. 1b) in order to compare the states of stress and strain, and the accumulation of damage in both processes. This specific application follows the work previously done by the authors (Centeno et al., 2016) although other analytical models like that of Wu et al. (2010) could have been used if the objective was solely focused on the distribution of strain and prediction of wall thickness.

2.2. Membrane equilibrium equations

The derivation of the membrane equilibrium equations in the circumferential, thickness and meridional directions entails a force balance in the local shell element ABCD with varying thickness (Fig. 1). The procedure gives rise to differential equations that are simplified using appropriate mathematical and physical assumptions.

2.2.1. Circumferential direction

The force balance in the circumferential direction gives (Fig. 1d),

$$\sigma_\theta\, r_1 d\alpha \left(t + \frac{dt}{2}\right) - \mu_\theta \sigma_t\, r_1 d\alpha \left(r + \frac{dr}{2}\right) d\theta - (\sigma_\theta + d\sigma_\theta)\, r_1 d\alpha \left(t + \frac{dt}{2}\right) = 0 \tag{1}$$

By neglecting higher order terms and considering circumferential friction stress $\mu_\theta \sigma_t$ to be applied at the centre of the local shell element, one obtains

$$d\sigma_\theta = -\mu_\theta \sigma_t \frac{r d\theta}{t} \cong -\mu_\theta \sigma_t \tag{2}$$

The simplification in Eq. (2) is based on the assumption that the width of the contact area is of approximately the same size as the tube wall thickness.

2.2.2. Thickness direction

The force balance in the thickness direction gives (Fig. 1d),

$$\sigma_t\, r\, d\theta\, r_1\, d\alpha + \sigma_\phi\, r\, d\theta\, t \sin\frac{d\alpha}{2} + (\sigma_\phi + d\sigma_\phi)(r + dr)\, d\theta\, (t + dt) \sin\frac{d\alpha}{2} + \\ + \sigma_\theta\, r_1\, d\alpha\, t \sin\frac{d\theta}{2}\cos\alpha + (\sigma_\theta + d\sigma_\theta)\, r_1\, d\alpha\, t \sin\frac{d\theta}{2}\cos\alpha = 0 \tag{3}$$

By neglecting higher order terms, taking $r_2 = r/\cos\alpha$ from Fig. 1c and substituting $d\sigma_\theta \cong -\mu_\theta \sigma_t$ from Eq. (2), the force balance can be expressed as,

$$\sigma_t \left(\frac{1}{t} - \frac{\mu_\theta}{2r_2}\right) + \frac{\sigma_\phi}{r_1} + \frac{\sigma_\theta}{r_2} = 0 \tag{4}$$

Further simplification of Eq. (4) based on $\mu_\theta / 2\, r_2 << 1/t$ allows neglecting the second term inside the brackets. In physical terms this means neglecting the influence of the circumferential friction stress $\mu_\theta \sigma_t$ in the force balance.

2.2.3. Meridional direction

The force balance in the meridional direction gives (Fig. 1d),

$$(\sigma_\phi + d\sigma_\phi)(r + dr)\, d\theta\, (t + dt) - \sigma_\phi\, r\, d\theta\, t + \mu_\phi\, \sigma_t\, r\, d\theta\, r_1\, d\alpha \\ - \sigma_\theta \sin\frac{d\theta}{2} r_1\, d\alpha\, t \sin\alpha - (\sigma_\theta + d\sigma_\theta) \sin\frac{d\theta}{2} r_1\, d\alpha\, t \sin\alpha = 0 \tag{5}$$

In the above equation $\mu_\phi \sigma_t$ is the meridional friction stress and the term involving $d\sigma_\theta \cong -\mu_\theta \sigma_t$ (Eq. (2)) is related to the projection of the circumferential friction stress along the meridional direction.

After neglecting higher order terms and taking $dr = r_1\, d\alpha \sin\alpha$, $r >> t \sin\alpha$ and $\mu_\theta / 2\, r << 1$ into consideration, one obtains,

$$\frac{d\sigma_\phi}{dr} + \frac{\sigma_\phi - \sigma_\theta}{r} + \frac{\mu_\phi\, \sigma_t}{t \sin\alpha} + \frac{\sigma_\phi}{t}\frac{dt}{dr} = 0 \tag{6}$$

Because the influence of the circumferential friction stress $\mu_\theta \sigma_t$ is once again absent from the final simplified equation, the friction coefficient μ will be hereafter exclusively associated to the meridional direction, e.g. $\mu \cong \mu_\phi$.

2.3. Analytical model for incremental tube expansion

The analytical model for incremental tube expansion is built upon the solution of the membrane equilibrium differential equations using pertinent simplifications and boundary conditions.

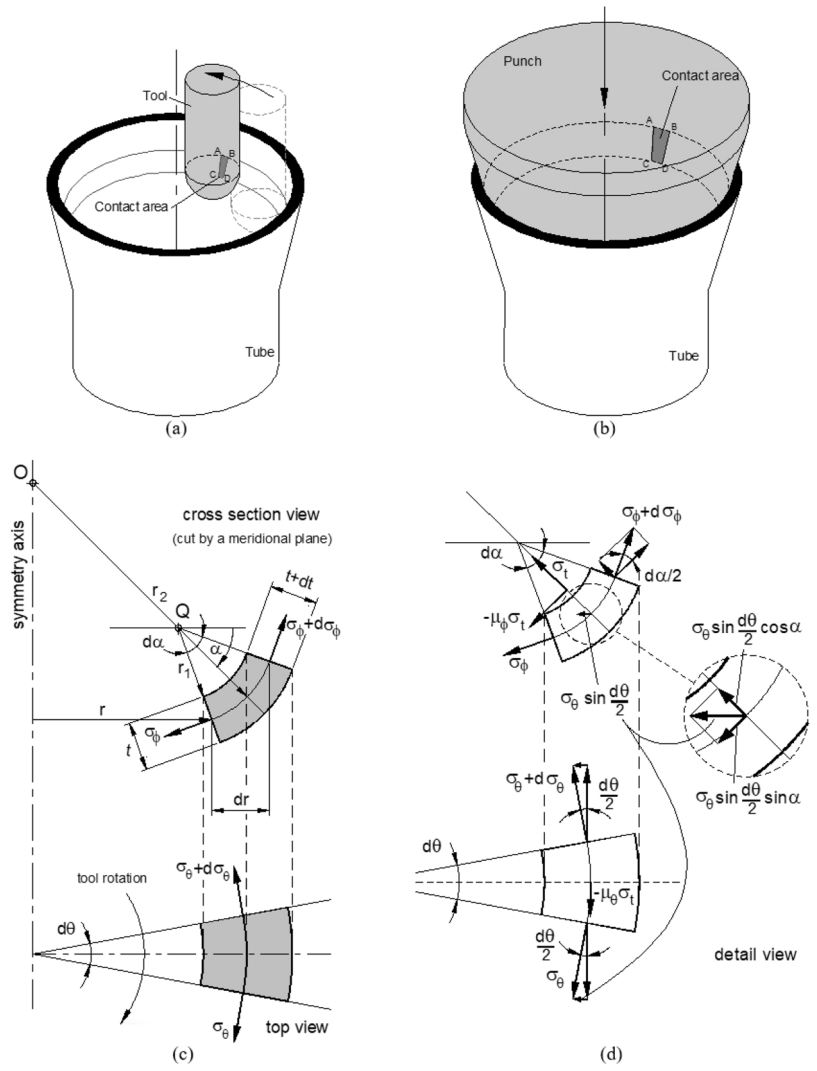

Fig. 1. Main schemes and notation utilized in the derivation of the analytical model. (a)Incremental tube expansion with a single point hemispherical punch; (b) Conventional tube expansion with a rigid tapered conical punch; (c) Shell element characteristic of the contact area between the tube and the tool/punch after being cut by an axial meridional plane; (d) Shell element characteristic of the contact area between the tube and the tool/punch with the applied stresses.

The derivation starts by substituting the geometrical condition $r_2 >> r_1$ in Eq. (4) and rearranging terms, to obtain the following relation between thickness and meridional stresses,

$$\sigma_t = -\sigma_\phi \frac{t}{r_1} = -\sigma_\phi \frac{t}{r_{tool}} \tag{7}$$

Eq. (7) allows concluding that the thickness stress σ_t is compressive and close to zero $|\sigma_t| \cong 0$ because the meridional stress σ_ϕ in incremental tube expansion is tensile, the thickness stress $\sigma_t = 0$ on the outside tube surface and $t/r_{tool} << 1$. Consequently, plane stress loading conditions are considered to prevail in the contact area between the tube and the single point hemispherical tool.

Now, by taking into consideration the experimental observations and measurements that revealed that incremental tube expansion is carried out under bi-axial stretching, and considering the Tresca yield criterion under rigid-perfectly plastic material assumptions $\sigma_\phi - \sigma_t = \sigma_Y$, the principal stresses in the contact area are

$$\begin{aligned} &\sigma_\phi = \sigma_1 \cong \sigma_Y > 0 \\ &\sigma_\theta = \sigma_2 \cong \gamma\sigma_1 > 0 \\ &\sigma_t = \sigma_3 \cong 0 \end{aligned} \tag{8}$$

where $\gamma = \sigma_\theta/\sigma_\phi$ is the ratio between circumferential and meridional stresses.

Fig. 2a presents a graphical representation of the stress field in a radial slice through the contact area between the tube and the single point hemispherical tool. As seen, the stresses have constant values and σ_θ differs from $\sigma_\phi = \sigma_Y$ as the stress ratio γ deviates from equal bi-axial stretching ($\gamma = 1$).

The stress ratio γ may be related to ratio $\beta = d\varepsilon_\theta/d\varepsilon_\phi$ of the plastic strain increments by application of the Levy-Mises constitutive equations,

$$\gamma = \frac{2\beta + 1}{2 + \beta} \tag{9}$$

The applied loading is assumed to be proportional so that $\beta = d\varepsilon_\theta/d\varepsilon_\phi = \varepsilon_\theta/\varepsilon_\phi$ coincides with the inverse of the strain path slope in principal strain space. Because the actual strain ratio β corresponding to bi-axial stretching is dependent on process parameters (e.g. the inclination of the tube wall) and bounded by the extreme plane strain $\beta = 0$ and equal bi-axial stretching $\beta = 1$ conditions, it follows from Eq. (9) that typical values of the stress ratio γ for incremental tube expansion are likely to vary in the range $0.5 < \gamma \leq 1$.

Considering the damage function proposed by Atkins (1996) that relates crack opening in tension (Mode I of fracture mechanics) and stress triaxiality $\sigma_m/\bar{\sigma}$ with the void growth model due to McClintock (1968),

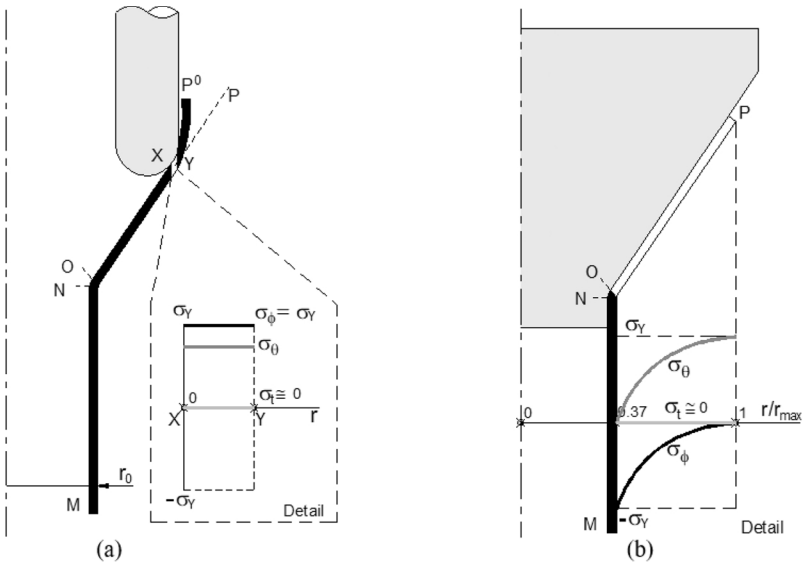

Fig. 2. Stress distribution in a radial slice through the instantaneous contact area between the tube and the tool/punch. (a)Incremental tube expansion; (b)Conventional tube expansion.

$$D_{crit} = \int_0^{\bar{\varepsilon}^f} \left(\frac{\sigma_m}{\bar{\sigma}}\right) d\bar{\varepsilon} \tag{10}$$

it is possible to express the critical ductile damage D_{crit} as a simple and easy-to-use function of the strain ratio β. This is accomplished by applying the effective stress $\bar{\sigma}$, the effective strain increment $d\bar{\varepsilon}$ (according to the von Mises yield criterion)

$$\bar{\sigma} = \sqrt{\sigma_\phi^2 + \sigma_\theta^2 - \sigma_\phi \sigma_\theta} \qquad d\bar{\varepsilon} = \frac{2}{\sqrt{3}} \sqrt{d\varepsilon_\phi^2 + d\varepsilon_\theta^2 + d\varepsilon_\phi d\varepsilon_\theta} \tag{11}$$

and the Levy-Mises constitutive equations to rewrite stress triaxiality and effective strain $\bar{\varepsilon}$, under plane stress $\sigma_t = 0$ loading conditions, as proposed by Martins et al. (2014),

$$\frac{\sigma_m}{\bar{\sigma}} = \frac{1}{\sqrt{3}} \frac{1+\beta}{\sqrt{1+\beta+\beta^2}}$$
$$\bar{\varepsilon} = \frac{2}{\sqrt{3}} \sqrt{1+\beta+\beta^2}\, \varepsilon_\phi \tag{12}$$

The simpler form of critical ductile damage D_{crit} resulting from substituting Eq. (12) into (10) is given by,

$$D_{crit} = \int_0^{\bar{\varepsilon}^f} \left(\frac{\sigma_m}{\bar{\sigma}}\right) d\bar{\varepsilon} = \int_0^{\bar{\varepsilon}^f} \frac{2}{3}(1+\beta)\, d\varepsilon_\phi = \frac{2}{3}(1+\beta)\, \varepsilon_\phi^f \tag{13}$$

where the superscript 'f' denotes fracture.

The critical ductile damage D_{crit} at the onset of fracture for incremental tube expansion will be obtained by substituting the experimental strain measurements in Eq. (13). This will be done in 'Results and Discussion'.

2.4. Analytical model for conventional tube expansion

A similar approach was utilized to obtain the states of stress and strain, and the accumulation of damage in conventional tube expansion. The main objective of including this other process is to provide a reference for better understanding the specificities of incremental tube expansion.

The derivation of the analytical model for conventional tube expansion starts by substituting the geometrical condition $r_1 = \infty$ imposed by the tapered conical punch in Eq. (4) and rearranging terms, to obtain the following relation between thickness and circumferential stresses (Fig. 1b and 1c),

$$\sigma_t = -\sigma_\theta \frac{t}{r_2} \tag{14}$$

Because the circumferential stress σ_θ in conventional tube expansion is tensile and $t/r_2 << 1$, Eq. (7) allows concluding that the thickness stress σ_t is compressive but close to zero $|\sigma_t| \cong 0$, so that plane stress loading conditions can also be considered to prevail in the contact area between the tube and the punch.

Recalling the simplified equilibrium Eq. (6) in the meridional direction and neglecting frictional effects $\mu\sigma_t \cong 0$ and variation in thickness $dt/dr \cong 0$, one obtains,

$$\frac{d\sigma_\phi}{dr} + \frac{\sigma_\phi - \sigma_\theta}{r} = 0 \tag{15}$$

Noting that the meridional stress σ_ϕ in conventional tube expansion is compressive, the term $\sigma_\theta - \sigma_\phi = \sigma_Y$ is constant and equal to the tube yield stress σ_Y according to Tresca yield criterion, under rigid-perfectly plastic material assumptions. This allows integrating Eq. (15) and writing the meridional stress σ_ϕ along the contact area between the tube and the punch, after substituting the boundary condition $\sigma_\phi = 0$ at the tube end $r = r_P$ (Fig. 2b) as

$$\sigma_\phi = \sigma_Y \ln\left(\frac{r}{r_P}\right) \tag{16}$$

Consequently, the state of stress along the contact area between the tube and the punch may be expressed as

$$\sigma_\theta = \sigma_1 = \sigma_Y \left(1 + \ln\frac{r}{r_P}\right) > 0$$
$$\sigma_t = \sigma_2 \cong 0$$
$$\sigma_\phi = \sigma_3 = \sigma_Y \ln\frac{r}{r_P} < 0 \tag{17}$$

Fig. 2b provides a schematic representation of the meridional σ_ϕ and circumferential σ_θ stresses in the contact area between the tube and the punch for the limiting expansion ratio r_0/r_{max} between the initial r_0 and final radius $r_P = r_{max}$. As seen, in contrast to incremental tube expansion that provides constant stresses along the instantaneous contact area, conventional tube expansion gives rise to logarithmic stress evolutions constrained by the limiting boundary conditions at the beginning $\sigma_\theta = 0$ ($r = r_0$) and end $\sigma_\phi = 0$ ($r = r_P$) of the expanded tube surface.

The limiting expansion ratio r_0/r_{max} may be derived from Eq. (17) after imposing the physical boundary condition of preventing the tube

from expanding at when $\sigma_\theta = 0$ (the limiting boundary condition at the beginning of the expanded tube surface),

$$\sigma_\theta = \sigma_Y\left(1 + \ln\frac{r_0}{r_{\max}}\right) = 0 \quad \rightarrow \quad \frac{r_0}{r_{\max}} = e^{-1} \cong 0.37 \tag{18}$$

This result allows concluding that conventional expansion of rigid perfectly plastic tubes is limited by a ratio $r_0/r_{\max} = 0.37$ below which fracture will be triggered at the tube end $r = r_P$. This ratio is exclusive of conventional tube expansion and does not apply to incremental tube expansion.

The critical value of damage in conventional tube expansion is calculated by means of the same Eq. (13) that was utilized for incremental tube expansion because cracking is also triggered by tension (Mode I of fracture mechanics). The main difference to incremental tube expansion is the possibility of determining a theoretical estimate of the critical damage at fracture for rigid perfectly plastic tubes based on the limiting expansion ratio $r_0/r_{\max} \cong 0.37$. This is done by considering tube expansion with a rigid conical punch D_{crit} to be carried out under pure tension $\beta = -1/2$ in the circumferential direction (as will be later discussed in 'Results and Discussion') and provides to the following estimate,

$$D_{crit} = \int_0^{\bar{\varepsilon}^f}\left(\frac{\sigma_m}{\bar{\sigma}}\right)d\bar{\varepsilon} = \int_0^{\bar{\varepsilon}^f}\frac{2}{3}(1+\beta)\,d\varepsilon_\theta = \frac{1}{3}\ln\frac{r_{\max}}{r_0} \cong 0.33 \tag{19}$$

with $\bar{\varepsilon}^f = \varepsilon_\theta^f = \ln(r_{\max}/r_0)$.

3. Experimentation

3.1. Tube expansion tests

The experiments in incremental and conventional expansion of thin-walled tubes were performed on commercial AA6063-T6 aluminium tubes with an outer radius $r_0 = 20$ mm and a wall thickness $t_0 = 2$ mm.

The work on incremental tube expansion (Fig. 3a) was performed on a Deckel Maho CNC machining centre equipped with a single point hemispherical tool, a mandrel and a chuck. The chuck was utilized to fix the tubes against the mandrel in order to prevent sliding and rotation during incremental forming.

The expanded tube surface was gradually formed with a fixed semi-angle of inclination ψ by a hemispherical tool, as it is shown in Fig. 3a. The tool followed a bottom-top spiral tool path that was generated in the commercial software MasterCAM. A lubricant paste Weicon ASW 040 P was continuously supplied to the plastically deforming region in order to reduce friction at the contact area between the tube and the tool.

Table 1
Summary of the main operating conditions utilized in the tube expansion tests. Notation according to Fig. 3.

Incremental tube expansion	
Tool radius r_{tool}	5 mm
Pitch p	2 mm
Step down Δz	0.2 mm
Semi-angle of inclination ψ	15º
Feed rate	1000 mm/min
Conventional tube expansion	
Cross head speed	5 mm/min
Semi-angle of inclination ψ	15º
Slant height s	38 mm

The work on conventional tube expansion (Fig. 3b) made use of a pressing die set with a tapered conical punch that was installed on a hydraulic testing machine (Instron SATEC 1200 kN). The lubricant paste employed in incremental tube expansion was also utilized in conventional tube expansion to reduce friction along the slant height s of the punch.

Table 1 summarizes the main operating parameters utilized in both tube expansion tests.

3.2. Strain measurements

Strain measurements were performed with two different techniques; circle grid analysis (CGA) and digital image correlation (DIC). CGA was utilized in incremental tube expansion because the overall movement of the experimental setup resulting from CNC is incompatible with the utilization of DIC.

Consequently, a grid of circular dots with $a_0 = 1.5$ mm x $b_0 = 1.5$ mm spacing was electrochemically etched on the outer tube surfaces in order to allow meridional and circumferential strains to be determined from the changes in spacing between two adjacent dots,

$$\varepsilon_{\phi_i} = \ln\left[\frac{0.5(a_i + a_{i+1})}{a_0}\right]\varepsilon_{\theta_i} = \ln\left[\frac{0.5(b_i + b_{i+1})}{b_0}\right] \tag{20}$$

Two types of measurements were performed. Measurements at the

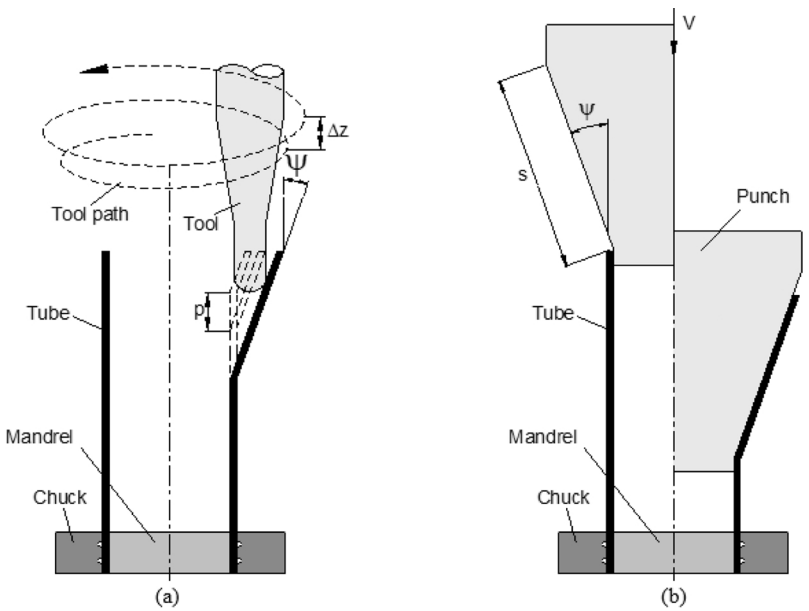

Fig. 3. Expansion of thin-walled tubes.(a)Schematic representation and notation of incremental tube expansion with a single point hemispherical tool (SPIF of tubes); (b)Schematic representation and notation of conventional tube expansion with a rigid tapered conical punch.

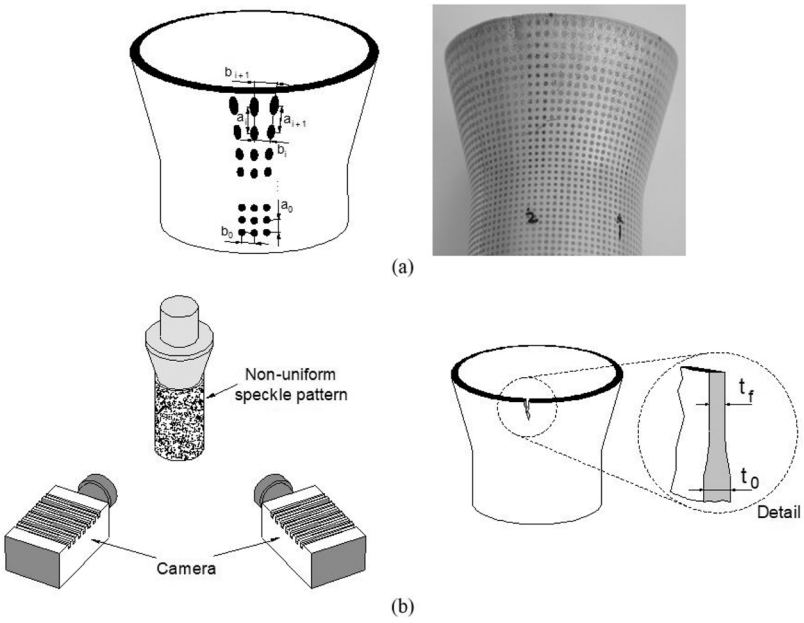

Fig. 4. Schematic representation of the strain measurement techniques utilized in the investigation. (a)Strain grid analysis for incremental tube expansion with representation of the grid utilized in the measurements; (b) Digital image correlation for conventional tube expansion complemented with measurements of the tube wall thickness at the crack to determine the gauge length strains at fracture.

vicinity of the tube end for different stages of the process in order to obtain the evolution of strain of a specific point (Fig. 4a), and measurements along the meridional direction of the expanded tube surface at the end of the process. The second type of measurements was necessary to construct the strain envelope in principal strain space, as will be shown in 'Results and Discussion'.

In case of conventional tube expansion, strain measurements were performed with a digital image correlation (DIC) system from Dantec Dynamics - model Q-400 3D (Fig. 4b). For this purpose, the surfaces of the tubes were sprayed with a stochastic black speckle pattern on a uniform background previously painted in white.

The utilization of DIC to characterize the state of strain up to the onset of necking followed a procedure recently developed by Cristino et al. (2018). However, its use to obtain the strains in the necks after they form and, therefore, close to fracture, provides values that cannot be considered the fracture strains due to the fact that such measurements suffer from sensitivity to the location of the selected points where measurements are to be performed owing to the inhomogeneous deformation in the neighbourhood of the crack. As a result of this, the experimental procedure for determining the fracture strains required measuring the tube wall thickness of the cracks with a stereomicroscope Nikon SMZ800 with a magnification of 20x to obtain the 'gauge length' strains. The procedure is schematically shown in Fig. 4b and the thickness strains at fracture ε_t^f ε_{tF} were calculated by,

$$\varepsilon_t^f = \ln \frac{t_f}{t_0} \tag{21}$$

where t_0 is the initial thickness and t_f $t_f = \frac{1}{n}\sum_{i=0}^{n} t_f^i$ the average thickness of the specimens at fracture. The meridional strain at fracture ε_ϕ^f is assumed to remain constant after the last measurement of DIC and the circumferential strain at fracture ε_θ^f is obtained by incompressibility under plane strain deformation conditions,

$$\varepsilon_\theta^f = -(\varepsilon_\phi^f + \varepsilon_t^f) \tag{22}$$

4. Results and discussion

4.1. Deformation mechanics

Fig. 5 presents the strain loading paths of a point located at the tube end for both conventional and incremental tube expansion processes. As seen, incremental tube expansion exhibits a near linear strain path with $\beta \cong 0.45$ radiating from the origin towards bi-axial stretching. Failure by fracture occurs for a thickness reduction $R = 100 \times (t_0 - t)/t_0$ of approximately 49 % without previous necking (refer to the black solid square marker in Fig. 5).

In contrast, conventional tube expansion exhibits a linear strain loading path that radiates from the origin with a ratio $\beta \cong -0.5$, typical of pure tension, up to localized necking. After necking, the strain loading path changes direction and becomes parallel to the major strain axis ($\beta = 0$, refer to the grey vertical dashed line in Fig. 5). Because AA6063-T6 is a very ductile material, there is a significant amount of straining between necking and fracture, which occurs for a thickness reduction $R \cong 37\%$ (refer to the grey solid circular markers in Fig. 5).

This difference in the strain loading paths indicates that fracture in incremental tube expansion is attained after a significant amount of thinning along the entire perimeter of the tube end whereas fracture in conventional tube expansion takes place by localized thinning within the necks that form at the tube end. However, both processes fail by crack opening in tension because incremental tube expansion is subjected to circumferential tensile stresses at the tube end and the localized necks that form in conventional tube expansion consist of plane strain necks along the meridional direction that experience thinning up to fracture by tensile stretching perpendicular to the neck

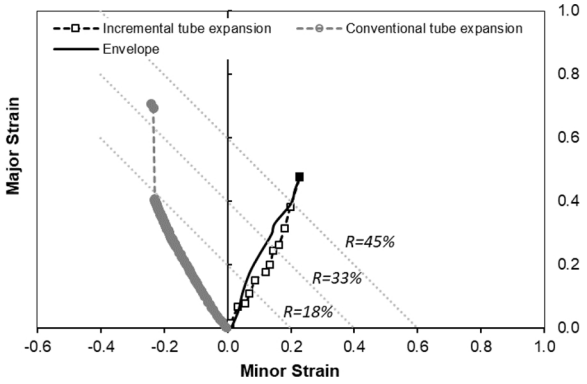

Fig. 5. Deformation history of a point located at the tube end for incremental tube expansion and conventional tube expansion. The black solid curve is the strain envelope and the dashed grey lines are the iso-thickness reduction (%) lines. The solid markers correspond to fracture.

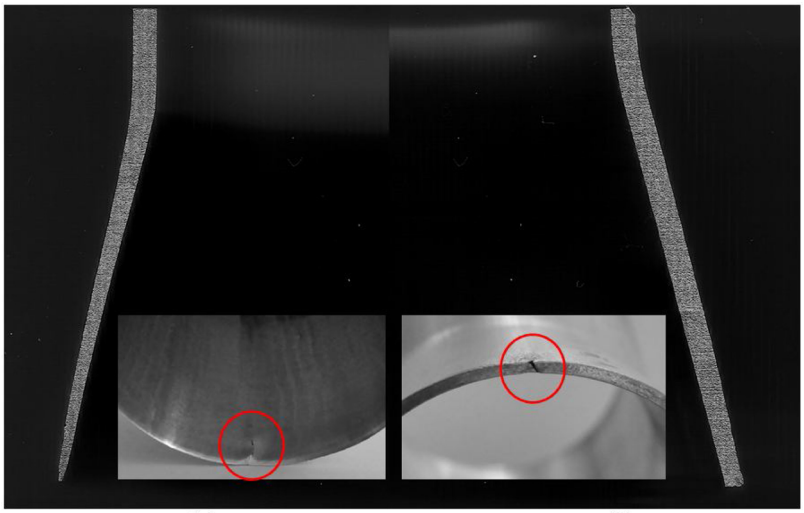

Fig. 6. Cross section of tubes subjected to (a) incremental and (b) conventional tube expansion.

(circumferential direction). No straining takes place along the necks.

The black solid line in Fig. 5 is the envelope of the greatest achievable strains resulting from all the strain paths of all the grid points located along the meridional direction of the expanded tube surface. The strain envelope was obtained from measurements performed after finishing the experiments on incremental tube expansion.

Because the differences between the strain envelope and the strain loading path of a point located at the tube end are minimum and because both evolutions are near linear, they allow validating the assumption of proportional loading that was included in the derivation of the analytical model (Section 2).

4.2. Damage

The critical damage at fracture D_{crit} for incremental tube expansion is determined by means of Eq. (13) after substituting the strain ratio β and the meridional strain at fracture ε_ϕ^f obtained from the experimental strain measurements (refer to the back solid square marker in Fig. 5),

$$\begin{aligned} &\beta \cong 0.45 \; \varepsilon_\phi^f = 0.48 \\ &D_{crit} = \frac{2}{3}(1+\beta)\varepsilon_\phi^f = 0.46 \end{aligned} \tag{23}$$

This value is significantly higher than the critical damage for conventional tube expansion of rigid perfectly plastic materials $D_{crit} \cong 0.33$ given by Eq. (19).

There are two main reasons justifying this difference. Firstly, the AA6063-T6 aluminium tube is not rigid perfectly plastic and, therefore, is not constrained by the theoretical limiting expansion ratio $r_0/r_{\max} \cong 0.37$.

Secondly, conventional tube expansion, in contrast to incremental tube expansion, experiences localized necking before fracture. This means that straining by tensile circumferential stresses applied in the direction perpendicular to the neck needs to be considered in case of conventional tube expansion and requires integration of Eq. (19) to be separated in two terms,

$$D_{crit} = \int_0^{\bar{\varepsilon}^f} \left(\frac{\sigma_m}{\bar{\sigma}}\right) d\bar{\varepsilon} = \int_0^{\varepsilon_\theta^n} \frac{2}{3}(1+\beta)\, d\varepsilon_\theta + \int_{\varepsilon_\theta^n}^{\varepsilon_\theta^f} \frac{2}{3}\, d\varepsilon_\theta \tag{24}$$

The first term corresponds to the strain loading path up to the onset of necking ε_θ^n, which is experimentally performed under near pure tension $\beta \cong -0.56$. The second term corresponds to the amount of straining from necking to fracture and is performed under plane strain deformation conditions $\beta = 0$.

Replacing the experimental data of Fig. 5 into Eq. (24), it is possible to determine the critical damage at fracture $D_{crit} = 0.32$ for the AA6063-T6 aluminium tubes subjected to real conventional expansion conditions. Because this value is similar to the theoretical critical damage $D_{crit} \cong 0.33$ (19) of a rigid perfectly plastic tube experiencing uniform thinning until fracture in conventional expansion, it may be concluded that the differences in critical damage D_{crit} are not due to the existence or non-existence of localized necking before cracking.

In fact, the higher value of critical damage at fracture for incremental tube expansion only reveals that the formability limit of the tubular material increases in first quadrant of the principal strain space. This result is consistent with the observation that the formability limit by fracture in principal strain space is not a straight line falling from left to right with slope '-1' (parallel to the iso-thickness reduction lines 'R') but a line with an 'upward curvature' tail in the first quadrant, as it was proposed by Martins et al. (2014). The consequence of this is that strains at fracture in incremental tube expansion are higher than in conventional tube expansion.

4.3. Thickness

Fig. 6 shows cross section photographs of tubes that were formed by incremental and conventional expansion. As seen, the tube subjected to incremental expansion reveals progressive wall thinning up to the end where fracture is triggered whereas that subjected to conventional expansion presents less wall thinning.

The justification for these differences is two-fold. Firstly, in incremental tube expansion the instantaneous contact area between the tube and the single point hemispherical tool is subjected to bi-axial stretching (Fig. 2a) whereas in conventional tube expansion the contact area between the tube and the punch is subjected to circumferential stresses $\sigma_\theta > 0$ that present a logarithmic evolution towards pure tension at the tube end (Fig. 2b). This means that the decrease in thickness t in conventional tube expansion tends to balance the increase in circumferential stress so that the resultant tension $T_\theta = \sigma_\theta t$ is approximately constant. This type of balance is commonly found in sheet metal forming processes (Marciniak and Duncan, 1992).

Secondly, in incremental tube expansion fracture takes place after a significant amount of thinning whereas in conventional tube expansion fracture occurs in localized necks undergoing significant local thinning (refer to the photographic detail in Fig. 6b).

The abovementioned differences in tube wall thickness are quantified in Fig. 7 that shows experimental measurements along the meridional

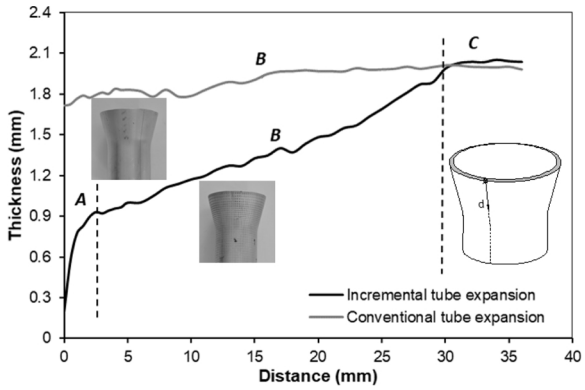

Fig. 7. Evolution of tube wall thickness with displacement measured along the meridional direction for incremental and conventional tube expansion. The measurements are performed from the tube end up to a position where both tubes were not subjected to deformation.

direction for the two different tube expansion processes. Three main regions may be distinguished in case of incremental tube expansion; (i) the region labelled as '*A*', located near the tube end (where distance *d* is zero), which is characterized by a sharp decrease in wall thickness, (ii) the region labelled as '*B*' where the wall thickness progressively increases as the distance to the tube end increases and (iii) the region labelled as '*C*' that corresponds to the tube not subjected to expansion.

These three regions are reduced to only two in case of conventional tube expansion because there is no region '*A*' due to progressive thinning in region '*B*' under a much smaller rate than that observed in incremental tube expansion. The sharp decrease in wall thickness (region '*A*') is a localized phenomenon that occurs inside the necks where fracture is triggered after a substantial amount of straining (refer to the close-up in Fig. 6b).

A close inspection of the tube produced by incremental expansion reveals that the sharp decrease in wall thickness associated to region '*A*' of Fig. 7 is linked to the occurrence of micro-cracks along the entire tube end perimeter. This is shown in the close-up photograph of Fig. 6a (refer to the ellipse) and justifies the reason why experimental strain measurements in incremental tube expansion where taken at approximately 3 mm from the tube end.

5. Conclusions

This paper presents an analytical model built-on membrane analysis that explains the deformation mechanics of incremental tube expansion. The model provides the distribution of stress in the instantaneous plastically deforming region corresponding to the contact area between the tube and the single point hemispherical tool as a function of the ratio between the circumferential and meridional stresses, and explains the physics behind failure by cracking. The actual ratio between the circumferential and meridional stresses is obtained from the experimental strain loading path in principal strain space.

Comparison with conventional tube expansion allows concluding that cracking takes place differently and after a significant and uniform amount of thinning at the tube end. This means that contrary to conventional tube expansion there is no development of necks at the tube end inside which fracture will be triggered after a substantial amount of localized straining.

Estimates of the accumulated ductile damage for both tube expansion processes indicate that formability is higher in case of incremental tube expansion. This is the result of strain loading paths being in the first quadrant of principal strain space where fracture limit curves often present upward curvature tails, as it was shown by Martins et al. (2014).

Author contributions section

V.A. Cristino: Conceptualization, Methodology, Investigation, Data Curation, Visualization, Funding acquisition

J.P. Magrinho: Investigation, Resources, Writing - Review & Editing

G. Centeno: Methodology, Investigation, Writing - Review & Editing,

M.B. Silva: Methodology, Investigation, Writing - Review & Editing,

P.A.F. Martins: Conceptualization, Methodology, Writing- Original draft preparation, Supervision, Funding acquisition

Declaration of Competing Interest

The authors declare that they have no known competing financial interests or personal relationships that could have appeared to influence the work reported in this paper.

Acknowledgments

The authors would like to acknowledge the support provided by Fundação para a Ciência e a Tecnologia of Portugal and IDMEC under LAETA-UID/EMS/50022/2019. Valentino Cristino would like to acknowledge the support provided by the Science and Technology Development Fund of Macao (grant no. 164/2017/A).

References

Atkins, A.G., 1996. Fracture in forming. Journal of Material Processing Technology 56, 609–618.
Centeno, G., Silva, M.B., Alves, L.M., Vallellano, C., Martins, P.A.F., 2016. Towards the characterization of fracture in thin-walled tube forming. Int. J. Mech. Sci. 119, 12–22.
Cristino, V.A.M., Magrinho, J.P.G., Silva, M.B., Centeno, G., Martins, P.A.F., 2018. A digital image correlation based methodology to characterize formability in tube forming. J. Strain Anal. Eng. Des in press.
Duflou, J.R., Habraken, A.M., Cao, J., Malhotra, R., Bambach, M., Adams, D., Vanhove, H., Mohammadi, A., Jeswiet, J., 2018. Single point incremental forming: state-of-the-art and prospects. Int. J. Mater. Form. 11, 743–773.
Kalpakjian, S., Rajagopal, S., 1982. Spinning of tubes: a review. J. Appl. Metalwork. 2, 211–223.
Marciniak, Z., Duncan, J.L., 1992. The Mechanics of Sheet Metal Forming. Edward Arnold, London.
Martins, P.A.F., Bay, N., Tekkaya, A.E., Atkins, A.G., 2014. Characterization of fracture loci in metal forming. Int. J. Mech. Sci. 83, 112–123.
Matsubara, S., 1994. Incremental nosing of a circular tube with a hemispherical head tool. J. Jpn. Soc. Technol. Plast. 35, 256–261.
McClintock, F.A., 1968. A criterion for ductile fracture by the growth of holes. Journal of Applied Mechanics – Transactions of ASME 35, 363–371.
Movahedinia, H., Mirnia, M.J., Elaysi, M., Baseri, H., 2018. An investigation on flaring process of thin-walled tubes using multistage single point incremental forming. Int. J. Adv. Manuf. Technol. 94, 867–880.
Silva, M.B., Skjoedt, M., Atkins, A.G., Bay, N., Martins, P.A.F., 2008a. Single point incremental forming & formability/failure diagrams. J. Strain Anal. Eng. Des. 43, 15–36.
Silva, M.B., Skjoedt, M., Martins, P.A.F., Bay, N., 2008b. Revisiting the fundamentals of single point incremental forming by means of membrane analysis. Int. J. Mach. Tools Manuf. 48, 73–83.
Teramae, T., Manabe, K., Ueno, K., Nakamura, K., Takeda, H., 2007. Effect of material properties on deformation behavior in incremental tube-burring process using a bar tool. Journal of Material Processing Technology 191, 24–29.
Wen, T., Yang, C., Zhang, S., Liu, L.T., 2015. Characterization of deformation behavior of thin-walled tubes during incremental forming: a study with selected examples. Int. J. Adv. Manuf. Technol. 78, 1769–1780.
Wen, T., Zheng, J., Qing, J., Fang, J., 2017. Outwards and inwards crimping of tube ends by single-point incremental forming. Procedia Eng. 207, 854–859.
Wu, W., Huang, Y., Malhotra, R., Wang, Y., Cao, J., 2010. Experimental and numerical analysis of titanium microtube elliptical flaring. In: Proceedings of the ASME 2010 International Manufacturing Science and Engineering Conference MSEC2010. Pennsylvania, USA. pp. 669–676.